Research Square

Preprints are preliminary reports that have not undergone peer review.
They should not be considered conclusive, used to inform clinical practice,
or referenced by the media as validated information.

A Surface-Imprinted Fluorescent Sensor Exploiting CsPbBr3@ZIF-8 for Selective and Sensitive Detection of Dopamine

Yaowei Qin
Jiangsu University
Junpeng Yang
Beijing Yongxin Environmental Protection Co., Ltd
Yijie Zhu
Department of Critical Care Medicine, Shanghai Tenth People's Hospital, School of Medicine, Tongji University, Shanghai 200072, P. R. China
Zhuanxi Zhang
Jinjiang Hospital of Traditional Chinese Medicine, Fujian University of Traditional Chinese Medicine
Jixiang Wang
Jiangsu University
Jingjing Xu
Department of Critical Care Medicine, Shanghai Tenth People's Hospital, School of Medicine, Tongji University, Shanghai 200072, P. R. China
Yue Ma
yamma@ujs.edu.cn
Jiangsu University

Research Article

Keywords: Dopamine, Molecularly imprinted polymer, Perovskite quantum dot, Fluorescence sensor, Parkinson's disease

Posted Date: November 12th, 2026

DOI: https://doi.org/10.21203/rs.3.rs-11441632/v1

License: This work is licensed under a Creative Commons Attribution 4.0 International License.
Read Full License

Additional Declarations: No competing interests reported.

A Surface-Imprinted Fluorescent Sensor Exploiting $CsPbBr_3$@ZIF-8 for Selective and Sensitive Detection of Dopamine

Yaowei Qin [a], Junpeng Yang [b], Yijie Zhu [c], Zhuanxi Zhang [d], Jixiang Wang [a*], Jingjing Xu [c*] and Yue Ma[a*]

[a] School of Chemistry and Chemical Engineering, Jiangsu University, Zhenjiang 212013, P. R. China

[b] Beijing Yongxin Environmental Protection Co., Ltd., Beijing 100020, P. R. China

[c] Department of Critical Care Medicine, Shanghai Tenth People's Hospital, School of Medicine, Tongji University, Shanghai 200072, P. R. China

[d] Emergency Department, Jinjiang Hospital of Traditional Chinese Medicine, Fujian University of Traditional Chinese Medicine, Quanzhou 362200, P. R. China

Corresponding Authors:

* yamma@ujs.edu.cn (Y. Ma)

* wjx@ujs.edu.cn (J. Wang);

* jingjing_xu@tongji.edu.cn (J. Xu)

* Dr. Jixiang Wang
E-mail address: wjx@ujs.edu.cn

* Prof. Jingjing Xu
E-mail address: jingjing_xu@tongji.edu.cn

* Prof. Dr. Yue Ma
E-mail address: yamma@ujs.edu.cn (Y. Ma)

Abstract

Accurate detection of dopamine (DA), a vital catecholamine neurotransmitter, is crucial for evaluating neurological functions and diagnosing related disorders. To address the challenges posed by complex biological matrices and trace DA concentrations, a robust fluorescent sensor was constructed by integrating molecularly imprinted polymers (MIPs) with ZIF-8-encapsulated $CsPbBr_3$ perovskite quantum dots ($CsPbBr_3$@ZIF-8@MIPs). In this rational design, the ZIF-8 shell serves as a protective barrier, effectively preventing $CsPbBr_3$ from degradation in polar solvents, while the surface-imprinted layer provides high-affinity and selective recognition sites for DA. The sensor exhibits a favorable linear response in the range of 5 – 400 nM, with an ultralow detection limit of 4.85 nM and a rapid response within 30s. When applied to clinical serum samples from Parkinson's disease patients, the sensor achieved satisfactory recoveries ranging from 96.83% to 109.72%, showing high consistency with the results obtained by high-performance liquid chromatography (HPLC). This work provides a reliable strategy for DA detection and demonstrates promising potential for biomedical sensing and clinical diagnosis.

Keywords: Dopamine，Molecularly imprinted polymer，Perovskite quantum dot，Fluorescence sensor, Parkinson's disease

Introduction

Dopamine (DA) is one of the most important catecholamine neurotransmitters in the central nervous system and plays a crucial role in regulating various physiological functions [1]. Notably, DA is involved in the pathogenesis of numerous neurological and psychiatric disorders, including Parkinson's disease, schizophrenia, and addiction, affecting millions of people worldwide [2]. For instance, Parkinson's disease impacts over 6 million individuals globally, many countries have established stringent standards for DA diagnosis, i.e. serum dopamine levels are typically around 0.1 - 0.5 μM in healthy individuals, may drop to < 0.1 μM in late stages of Parkinson's disease [3]. Therefore, accurate measurement of DA concentration in biological samples is essential for advancing neurological health monitoring and facilitating therapeutic interventions. Traditional techniques for DA analysis include enzyme-linked immunosorbent assay (ELISA), high-performance liquid chromatography (HPLC), and liquid chromatography–mass spectrometry (LC–MS) [4]. However, these methods often suffer from limitations such as complex pretreatment steps, high operational costs, lengthy analysis time, insufficient temporal resolution, and reliance on sophisticated instrumentation. In light of these constraints, there is an urgent need to develop simple, rapid, highly sensitive, and efficient analytical methods for the qualitative and quantitative assessment of DA [5].

In this context, fluorescent sensors have gained prominence for molecular detection due to their operational simplicity, visual signal output, and rapid response [6]. Various quantum dots (QDs), including CdTe, ZnS, and carbon quantum dots (CQDs), have been employed as fluorophores in the design of fluorescent probes for DA detection [7-9]. While these QDs exhibit satisfactory performance, many suffer from drawbacks such as low quantum yield, complicated synthesis procedures, and limited sensitivity [10] Inorganic halide perovskite quantum dots (IPQDs) have recently attracted significant attention owing to their excellent optical properties, high sensitivity, and high quantum yield [11, 12]. With their widespread application in optoelectronics, the use of IPQDs as fluorophores in molecular detection is rapidly advancing. However, a major challenge persists: IPQDs are highly susceptible to degradation in polar solvents, leading to rapid fluorescence quenching during detection [13]. As a result, most detection applications are conducted in non-polar, often toxic solvents, which severely limits their practical utility. Therefore, enhancing the aqueous

stability of IPQDs through modification or encapsulation has become a key research focus [14].

Recently, surface ligand engineering has achieved significant advances through the introduction of strong-binding ligands, polymer-based ligands, or the construction of superhydrophobic surfaces, thereby fundamentally enhancing the intrinsic stability of IPQDs [15-17]. However, relying solely on surface chemical modifications often proves insufficient for providing long-term and complete protection. In this context, metal–organic framework (MOF) encapsulation strategies have emerged as a promising next-generation approach for highly efficient stabilization [18, 19]. MOFs not only offer a robust, structurally designable physical barrier but also leverage their unique spatial confinement effect to suppress particle aggregation and ensure uniform size distribution. Their highly tunable architectures enable the development of "smart" protective shells with selective permeability, overcoming the limitations of traditional dense coatings that cause complete shielding. Among all MOF shells, ZIF-8 is particularly suitable for encapsulating IPQDs in this work because it enables mild aqueous synthesis, optimal pore confinement, water stability, and facile surface modification—advantages that many other MOFs (e.g., lanthanide-based MOFs) lack due to harsh synthesis conditions or poor water stability. Molecular recognition elements that can be modified on the surface of ZIF-8 include antibodies, aptamers, and enzymes [20]. However, biological recognition elements generally have limitations such as poor stability, high cost, and complex preparation. In contrast, molecularly imprinted polymers (MIPs) induce the polymerization of functional monomers to form three-dimensional cavities that precisely match the target in size, shape, and functional groups, exhibiting unique advantages: first, they have excellent selectivity and can specifically capture target molecules through multiple interactions, such as hydrogen bonding, π-π stacking, and boronic acid covalent bonds, effectively excluding interference from structurally similar molecules; second, MIPs possess outstanding physicochemical stability and reusability, with their cross-linked polymer structure resisting long-term storage and harsh environments; third, they are flexible to synthesize and cost-effective [21-23]. Thus, using MIPs as specific recognition shell may endow fluorescent sensors with significant signal out-put ability, which might be used as measurement method for the detection of the target molecule [24-26].

In this work, we designed a surface-imprinted fluorescent sensor based on ZIF-8 encapsulated $CsPbBr_3$ ($CsPbBr_3$@ZIF-8@MIPs) for effective recognition of DA through the synergistic effect of two functional monomers, namely acrylamide and 4-vinylphenylboronic acid, providing

high-affinity and selective recognition sites for DA via hydrogen bonds, π - π stacking and boric acid covalent interaction (Fig. 1) [27, 28]. After encapsulating IPQDs into ZIF-8, the resulting composite exhibits excellent optical properties and high sensitivity, with a response time of approximately 30 s toward DA. Moreover, owing to the large specific surface area of ZIF-8, the composite possesses strong adsorption capacity, achieving a detection limit as low as 4.8 nM. Detailed investigations are provided in the Discussion section.Furthermore, the surface-imprinted polymer layer imparts specific recognition capabilities, effectively minimizing interference from structurally similar compounds. The final fluorescent sensor, $CsPbBr_3$@ZIF-8@MIPs, is successfully applied for the detection of DA in human serum, demonstrating significant potential for practical applications in clinical diagnosis.

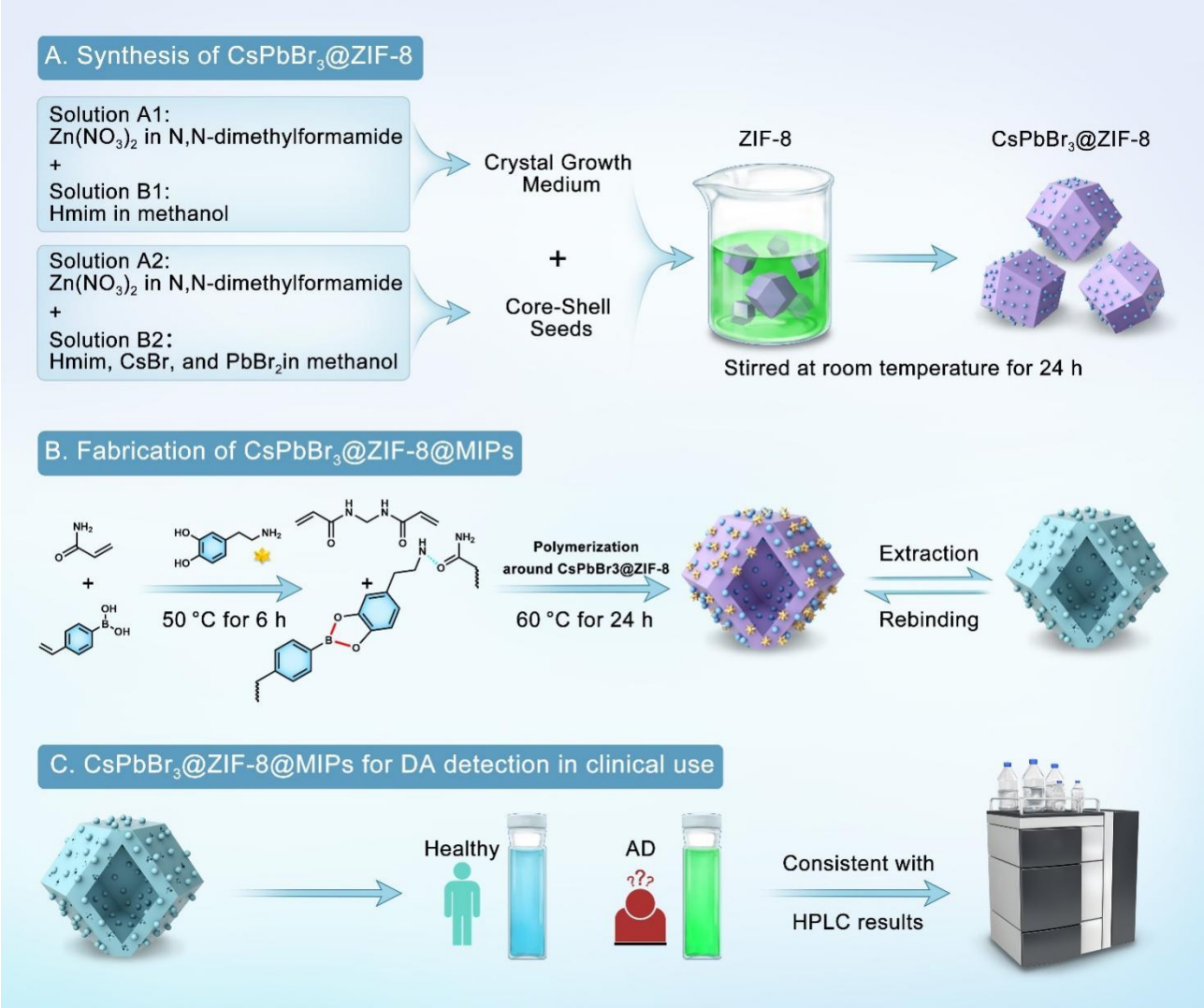


Fig. 1. Schematic illustration of fluorescent sensor $CsPbBr_3$@ZIF-8@MIPs synthesis and application.

Experimental

Reagents. All reagents used in this study were of analytical grade and employed without further purification. N,N-Dimethylformamide, methanol, $Zn(NO_3)_2 \cdot 6H_2O$, 2-methylimidazole (Hmim), $PbBr_2$, CsBr, acrylamide (AM), 2,2′-azobis(isobutyronitrile) (AIBN), N,N'-methylenebis(acrylamide) (MBAAM), and dopamine (DA) were purchased from Sinopharm Chemical Reagent Co., Ltd. (Shanghai, China).

Instruments: Fluorescence measurements were performed on an F98 fluorescence spectrophotometer (Shanghai Lengguang Technology Co., Ltd., China). Morphological characteristics were examined using scanning electron microscopy (SEM, JEOL JSM-7001F) and transmission electron microscopy (TEM, JEOL JEM-2100). The specific surface area was determined by a fully automated surface area and pore size analyzer (NOVA 3000e). Quantitative analysis of dopamine (DA) was carried out by high-performance liquid chromatography (HPLC, Agilent 1200 series, Agilent Technologies, USA) equipped with a UV-vis detector.

Synthesis of $CsPbBr_3$@ZIF-8. Solution A_1 was prepared by dissolving 300 mg of $Zn(NO_3)_2 \cdot 6H_2O$ in 10 mL of N,N-dimethylformamide. Another identical solution was labeled as Solution A_2. Solution B1 was obtained by dissolving 656 mg of Hmim in 10 mL of methanol. Solution B_2 was prepared by dissolving 656 mg of Hmim, 276 mg of CsBr, and 367 mg of $PbBr_2$ in 10 mL of methanol. Solution A_1 was then added to Solution B1 under ultrasonication for 5 minutes. Subsequently, Solution A_2 was poured into Solution B_2, and the resulting mixture was immediately added to the previously sonicated solution. The reaction mixture was stirred at room temperature for 24 h. After the reaction, the product was collected by centrifugation and dried, yielding $CsPbBr_3$@ZIF-8.

Synthesis of $CsPbBr_3$@ZIF-8@MIPs. A total of 50 mg of $CsPbBr_3$@ZIF-8 was added to a flask containing 50 mL of ethanol. Then, 5.7 mg of acrylamide (AM) and 12 mg of VPBA were introduced as functional monomers, along with 7.5 mg of DA as the template molecule. The mixture was stirred at 50 °C for 6 h. Subsequently, 54.2 mg of MBAAM was added as the cross-linker and 5.0 mg of AIBN as the initiator. The reaction system was purged with nitrogen for 30 minutes and then allowed to proceed at 60 °C for 24 h under continuous stirring. After polymerization, the product was collected by centrifugation and washed using a mixture of

methanol/acetic acid (9:1, v/v) as eluent in a Soxhlet extractor for 48 h. The final material was dried at 60 °C and denoted as $CsPbBr_3$@ZIF-8@MIPs. For comparison, a non-imprinted polymer ($CsPbBr_3$@ZIF-8@NIPs) was synthesized following the same procedure but in the absence of DA.

Detection of DA. A 1 mL aliquot of the sample (0.3 mg/L) was mixed with 2 mL of dopamine (DA) solutions at varying concentrations (ranging from 0 to 600 nM) at pH 7.0 (Figure S1). After incubation for a certain period, the fluorescence spectra were recorded within the range of 480–565 nm under an excitation wavelength of 365 nm.

Serum sample treatment. Serum samples were collected from healthy adult volunteers and Parkinson's patients by Shanghai Tenth People's Hospital (No. 24KN106). The blood samples were centrifuged, and the supernatant was collected for direct use.

HPLC detection. HPLC analysis was performed as the gold standard by using an Agilent Technologies 1200 system (Agilent, USA) equipped with a C18 reversed-phase column (4.6 × 150 mm, 4 μm) maintained at 298.15 K. The mobile phase consisted of potassium dihydrogen phosphate (0.1 mol/L) and methanol in a ratio of 85:15 (v/v), delivered at a flow rate of 1.0 mL/min. Detection was carried out at a wavelength of 280 nm.

Results and discussion

The synthesis process of $CsPbBr_3$@ZIF-8@MIPs is illustrated in Fig. 1. Initially, $CsPbBr_3$@ZIF-8 was prepared via an in-situ growth method. In this system, the green-emitting $CsPbBr_3$ quantum dots serve as the fluorescence signal source for DA detection, while ZIF-8 acts as the structural scaffold. Dopamine (DA) was used as the template molecule, with acrylamide (AAm) and 4-vinylphenylboronic acid (4-VPBA) employed as the backbone and functional monomers, respectively. N, N′-methylenebis(acrylamide) (MBAAm) was used as the cross-linker, and 2,2′-azobis(isobutyronitrile) (AIBN) as the initiator. The hydrophilic nature of AAm helps suppress nonspecific binding in human blood samples, while 4-VPBA enhances the specific recognition of DA through boronate–catechol interactions and B–N coordination. The combination of the porous structure of ZIF-8, the high sensitivity of $CsPbBr_3$ QDs, and the specific recognition provided by the imprinted layer enables highly sensitive and selective detection of DA.

Physicochemical property characterization. Fig. 2a presents the powder X-ray diffraction (PXRD) patterns of ZIF-8, pristine $CsPbBr_3$, and synthesized $CsPbBr_3$@ZIF-8 composite. The

pattern of pure ZIF-8 (black curve) exhibits characteristic sharp diffraction peaks, for instance, at 2θ values of 14.7°, 18°, 26.7° and 30°, which are in good agreement with the simulated pattern, confirming its highly crystalline nature. The pattern for the synthesized $CsPbBr_3$ (red curve) shows distinct peaks at approximately 21.5°, 30.5°,37.5 and 43.6°, indicative of its typical perovskite crystal structure. Notably, the PXRD pattern of the $CsPbBr_3$@ZIF-8 composite (blue curve) clearly comprises all the characteristic peaks of both ZIF-8 and $CsPbBr_3$ without the appearance of any additional impurity phases. This simultaneous presence of the distinctive diffraction features from both components provides conclusive evidence for the successful formation of a composite material in which the crystalline structures of $CsPbBr_3$ and ZIF-8 are well preserved.

Additionally, FT-IR spectroscopy confirmed the successful synthesis of $CsPbBr_3$@ZIF-8@MIPs (Fig. 2b). Characteristic vibrational peaks of $CsPbBr_3$@ZIF-8 were preserved, including C=N stretching band of imidazole rings at 1580 cm^{-1}, indicating structural integrity of the MOF. New absorption bands appeared at 1650 cm^{-1} (C=O stretch) and 1540 cm^{-1} (N-H bending), attributed to amide functionalities originating from acrylamide and the MBA crosslinker, thereby confirming polymerization around the ZIF-8 scaffold. Notably, the B-O stretching vibration of 4-vinylphenylboronic acid (VPBA) shifted from 1340 cm^{-1} in the free boronic acid form to 1380 cm^{-1} with significant peak broadening upon complexation, providing strong evidence for the formation of reversible boronate esters between the boronic acid moiety and catechol groups of the dopamine. The presence of a distinct B-O deformation peak at 660 cm^{-1} further corroborated the incorporation of VPBA into the polymer matrix. Collectively, these spectroscopic features confirm the successful fabrication of $CsPbBr_3$@ZIF-8@MIPs with specifically designed recognition sites.

As shown in Fig. 3a-d, the specific surface area, pore size distribution, and total pore volume of $CsPbBr_3$@ZIF-8, $CsPbBr_3$@ZIF-8@MIPs, and $CsPbBr_3$@ZIF-8@NIPs were analyzed by N_2 adsorption–desorption measurements. The Brunauer-Emmett-Teller (BET) surface area and total pore volume of $CsPbBr_3$@ZIF-8 were determined to be 843.607 m^2/g and 0.404 cm^3/g, respectively. For $CsPbBr_3$@ZIF-8@MIPs, these values increased to 856.382 m^2/g and 0.823 cm^3/g, whereas for $CsPbBr_3$@ZIF-8@NIPs, they significantly decreased to 345.978 m^2/g and 0.178 cm^3/g. These results suggest that the MIP forms a thin, porous shell on the surface of $CsPbBr_3$@ZIF-8 without blocking the internal pores of the ZIF-8 framework. Moreover, the notable increase in total pore

volume observed in $CsPbBr_3$@ZIF-8@MIPs can be attributed to the formation of abundant imprinting cavities after the removal of DA. On the other hand, $CsPbBr_3$@ZIF-8@NIPs have particularly low BET surface area and total pore volume due to the lack of imprinted cavities. This provides strong evidence for the successful fabrication of $CsPbBr_3$@ZIF-8@MIPs with well-preserved porosity and accessible binding sites.

The morphological characteristics of $CsPbBr_3$@ZIF-8,$CsPbBr_3$@ZIF-8@MIPs and $CsPbBr_3$@ZIF-8@NIPs were investigated using scanning electron microscopy (SEM) and transmission electron microscopy (TEM), showing a size around 150 nm, as illustrated in Fig. 3e-h. The SEM images reveal that $CsPbBr_3$@ZIF-8 maintains the dodecahedral structure of ZIF-8, with a smooth and well-defined surface. TEM analysis further reveals that $CsPbBr_3$@ZIF-8 exhibits a clear hexagonal morphology, excellent dispersity, and minimal agglomeration, confirming the successful integration of $CsPbBr_3$ within the ZIF-8 framework. These results highlight the effectiveness of ZIF-8 as a suitable supporting matrix. For $CsPbBr_3$@ZIF-8@MIPs, SEM images clearly show increased surface roughness after polymer coating. TEM images further show that the hexagonal shape is largely preserved, while the surface becomes noticeably rougher due to the presence of MIP layer. The layer has a uniform thickness of approximately 10 nm, and the material remains well-dispersed without significant aggregation, which is beneficial for enhancing adsorption capacity toward DA and improving detection sensitivity. Collectively, these observations provide strong evidence for the successful fabrication of $CsPbBr_3$@ZIF-8@MIPs with desirable structural and functional properties.

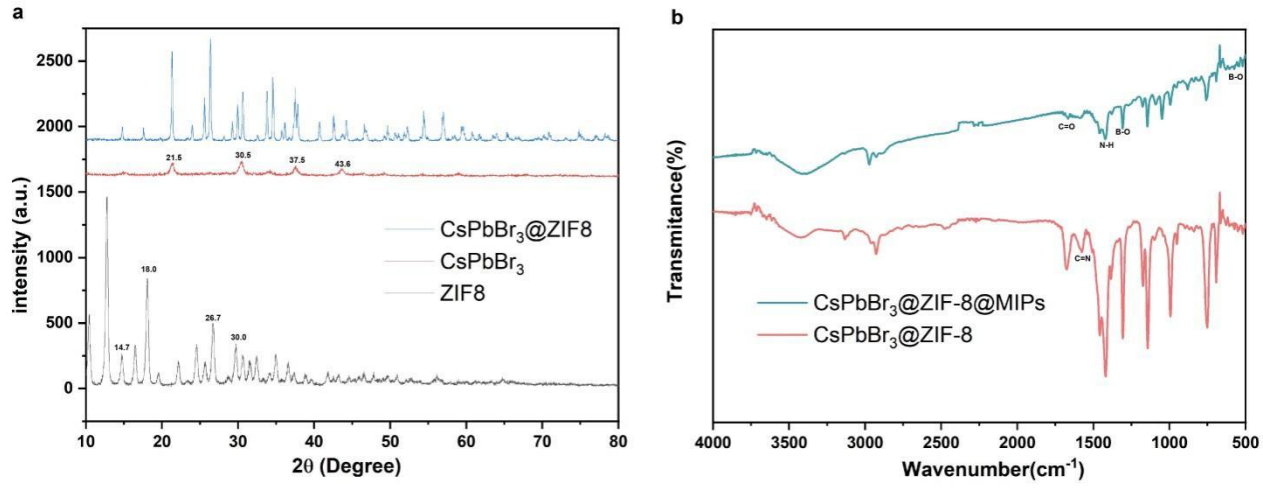
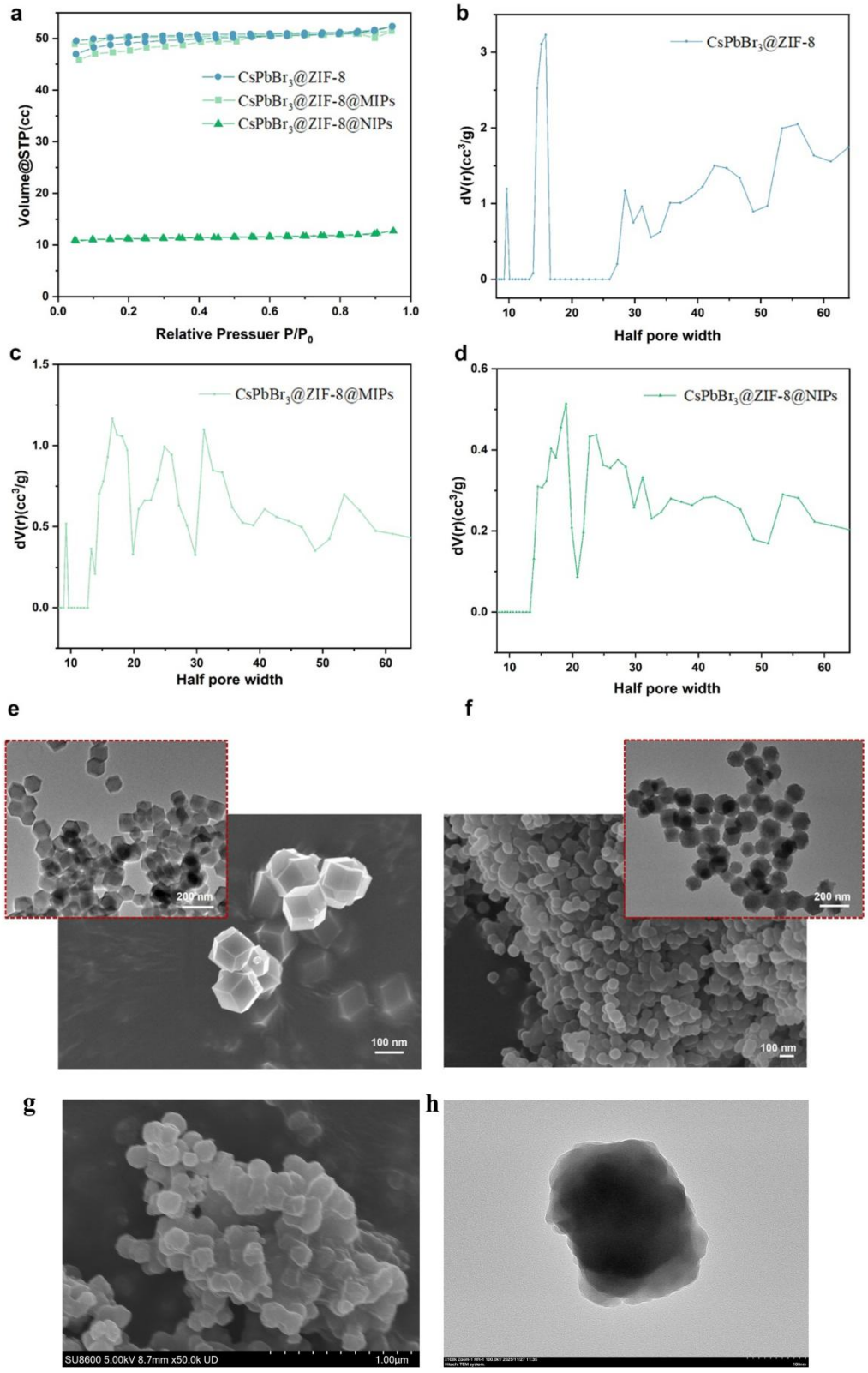


Fig. 2. Characterization of $CsPbBr_3$@ZIF-8 via XRD (a). Characterization of $CsPbBr_3$@ZIF-8@MIPs via FT-IR



(b).

Fig. 3. N_2 adsorption-desorption isotherm (a) and the corresponding pore size distributions (b,c,d) of different samples. SEM image (e) and TEM image (insert) of CsPbBr3@ZIF-8. SEM image (f) and TEM image (insert) of CsPbBr3@ZIF-8@MIPs .SEM image (g) and TEM image (h) of CsPbBr3@ZIF-8@NIPs.

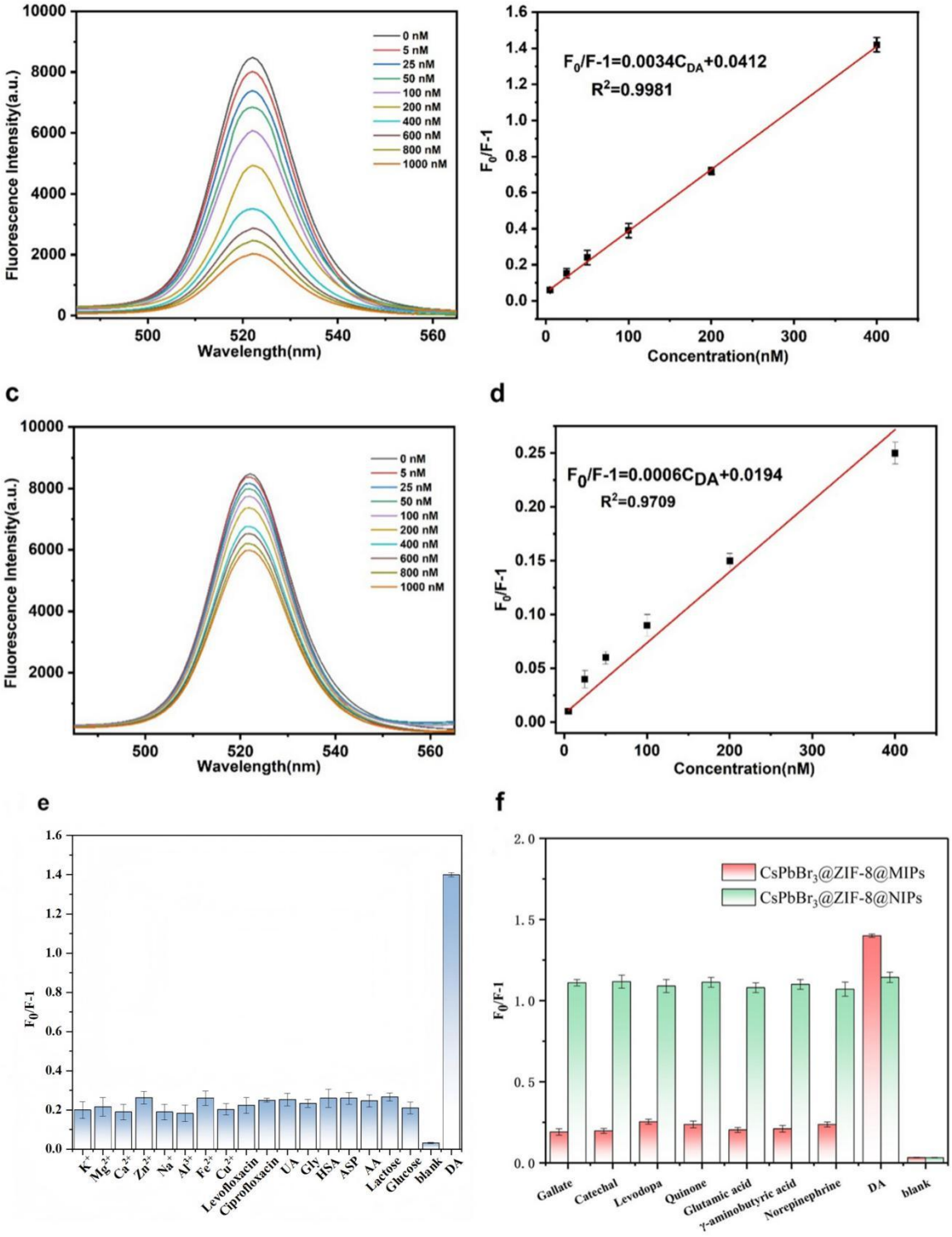


Fig. 4. Fluorescence spectra of $CsPbBr_3$@ZIF-8@MIPs (a) and $CsPbBr_3$@ZIF-8@NIPs (c) upon the exposure to different concentrations of DA. The fluorescence quenching rate and linear relationships of $CsPbBr_3$@ZIF-8@MIPs (b) and $CsPbBr_3$@ZIF-8@NIPs (d) upon the exposure to different concentrations of DA. Selectivity test of $CsPbBr_3$@ZIF-8@MIPs for determining DA with respect to common ions and organic molecules (e). Selectivity evaluation of $CsPbBr_3$@ZIF-8@MIPs and $CsPbBr_3$@ZIF-8@NIPs for recognizing DA and its structural analogs (f).

Detection performance evaluation. The fluorescence capability of $CsPbBr_3$@ZIF-8@MIPs is crucial for evaluating the sensor's detection performance. As shown in Fig. 4a-b, $CsPbBr_3$@ZIF-8@MIPs exhibits a distinct fluorescence emission peak at 522 nm, and its intensity decreases progressively with increasing dopamine (DA) concentration – demonstrating a clear fluorescence quenching effect. When the concentration of DA exceeds 400 nM, the extent of fluorescence quenching gradually plateaus. Notably, the quenching efficiency reaches saturation when the DA concentration exceeds 400 nM. A robust linear correlation is observed between the normalized quenching efficiency ($F_0/F - 1$) and DA concentration (C_{DA}) over the range of 5 – 400 nM, fitting the equation: $F_0/F - 1 = 0.0034C_{DA} + 0.0412$, with an excellent correlation coefficient (R^2) of 0.9981. Based on the standard limit of detection (LOD) formula (LOD = 3σ/k, where σ is the standard deviation of blank measurements and k is the slope of the calibration curve [29, 30]), the value is determined to be 4.85 nM. These results confirm that $CsPbBr_3$@ZIF-8@MIPs enables highly sensitive and quantitative detection of DA within the linear dynamic range of 5–400 nM. In contrast, the control material $CsPbBr_3$@ZIF-8@NIPs (prepared without DA templating) shows negligible fluorescence quenching even at elevated DA concentrations (Fig. 4c–d). Only marginal quenching is observed up to 600 nM DA, with a significantly weaker linear response described by: $F_0/F - 1 = 0.0006C_{DA} + 0.0194$, and a lower correlation coefficient ($R^2 = 0.9709$). The stark contrast in quenching behavior between MIPs and NIPs unambiguously verifies that DA acts as an efficient and selective quencher for $CsPbBr_3$@ZIF-8@MIPs – highlighting the critical role of molecular imprinting in conferring high specificity toward DA.

To evaluate the selectivity of $CsPbBr_3$@ZIF-8@MIPs, a panel of common biological interferents was tested, including 10 representative inorganic ions (K^+, Mg^{2+}, Ca^{2+}, Zn^{2+}, Na^+, Al^{3+}, Fe^{2+}, Cu^{2+}) and 7 organic species (uric acid [UA], glycine [Gly], human serum albumin [HSA], aspirin [ASP], ascorbic acid [AA], lactose, and glucose) commonly present in human blood, as well as two fluoroquinolone antibiotics (levofloxacin and ciprofloxacin). As shown in Fig. 4e, at a concentration of 10 times DA(1 μM), none of these interferents induced appreciable fluorescence quenching of $CsPbBr_3$@ZIF-8@MIPs. In stark contrast, DA alone triggered pronounced quenching, with a quenching efficiency of ~1.4, demonstrating exceptional specificity for DA over abundant physiological components. To further probe structural discrimination, we assessed a set of DA structural analogs: gallic acid, catechol, levodopa, benzoquinone, glutamic acid, γ-aminobutyric

acid, and norepinephrine. As illustrated in Fig. 4f, even at an equimolar concentration (100 nM), these analogs caused negligible fluorescence quenching, whereas DA maintained a consistently high quenching efficiency (~1.4). In comparison, $CsPbBr_3$@ZIF-8@NIPs showed responses to some structural analogs.Notably, levodopa and norepinephrine, two molecules sharing nearly identical catechol-amine motifs with DA, induced only minimal signal changes, underscoring the precise molecular recognition capability of the MIP cavities. These results collectively confirm that $CsPbBr_3$@ZIF-8@MIPs possesses highly specific binding sites tailored for DA, rendering it a promising platform for selective DA detection in complex biological matrices such as human blood.

Detection Mechanism. The sensitive and selective fluorescence quenching toward DA is attributed to synergistic specific molecular recognition and efficient signal transduction. The main quenching mechanism is photoinduced electron transfer (PET) from DA to $CsPbBr_3$ QDs.

Upon the specific rebinding of DA molecules into the imprinted cavities on the MIP shell, the electron-rich catechol groups of DA are brought into close proximity (within the Förster distance) to the surface of the $CsPbBr_3$ QDs. Under photoexcitation, electrons in the QDs are promoted from the valence band to the conduction band, generating excitons. Thermodynamically, the favorable alignment of energy levels—where the highest occupied molecular orbital of DA is higher than the valence band edge of $CsPbBr_3$—facilitates the transfer of an electron from DA to the photogenerated hole in the QDs. This non-radiative electron transfer process effectively competes with and suppresses the radiative recombination of excitons, resulting in a pronounced quenching of the QDs' fluorescence intensity.This PET process is essentially a dynamic competition between electron transfer and exciton radiative decay, where the rate of electron transfer is strongly dependent on the donor–acceptor distance and the orbital overlap integral.

Fig. 4b exhibits a good linear relationship in the low concentration range, which is characteristic of static quenching arising from the formation of a ground-state complex between the QD and the quencher (DA). The role of the MIP shell is crucial in this process; it not only provides selectivity but also pre-concentrates the DA analyte at the QD surface, creating an ideal microenvironment for efficient electron transfer.Therefore, we conclude that the fluorescence quenching is dominantly governed by a PET mechanism, which is initiated by the specific molecular recognition event and transduces it into a highly sensitive optical signal. The ZIF-8 interlayer further ensures the stability of the QD emitters, allowing this efficient PET process to be

reliably measured.Moreover, the confinement effect of the imprinted cavities not only enhances the local concentration of DA but also restricts the molecular orientation, thereby maximizing the orbital coupling efficiency between DA and the QD surface for optimal PET.

Stability, Reusability and Response Time. The stability of both $CsPbBr_3$@ZIF-8@MIPs and $CsPbBr_3$@ZIF-8@NIPs was evaluated over a 60-hour period, with fluorescence intensity measured at 5-hour intervals (Fig.5a). The fluorescence intensity of both materials remained nearly constant across all 13 measurements, demonstrating that $CsPbBr_3$@ZIF-8@MIPs maintains its structural integrity and functional performance during prolonged storage, thereby highlighting its excellent stability. Figure Fig.5b presents a detailed investigation of the pH effect on the performance of $CsPbBr_3$@ZIF-8@MIPs. It was found that DA could be detected under highly acidic or alkaline conditions; nevertheless, the most intense signal was achieved at pH 7. Hence, all subsequent experiments were conducted at pH 7 to ensure optimal analyte stability and detection efficiency. In addition, the reusability of $CsPbBr_3$@ZIF-8@MIPs was evaluated through six consecutive adsorption – desorption cycles (Fig.5c). The results demonstrated that the fluorescence intensity remained stable over the first five cycles with only a slight decline in the sixth cycle, indicating good regenerative performance and practical reusability of the material.

To investigate the optimal detection time of DA using $CsPbBr_3$@ZIF-8@MIP, 200 nM DA was introduced into the $CsPbBr_3$@ZIF-8@MIP system, and the fluorescence intensity was recorded at various time intervals. As illustrated in Fig.5d, the fluorescence intensity of the detection solution underwent a rapid decrease within the first 30 seconds, after which it reached a plateau and remained stable. This swift detection performance is attributable to the high sensitivity of the IPQDs, the strong adsorption capacity of ZIF-8, and the rapid adsorption and binding of DA with the recognition sites on the thin-layer surface-imprinted nanoshell. Consequently, 30 s was chosen as the optimal measurement time for subsequent fluorescence assays.

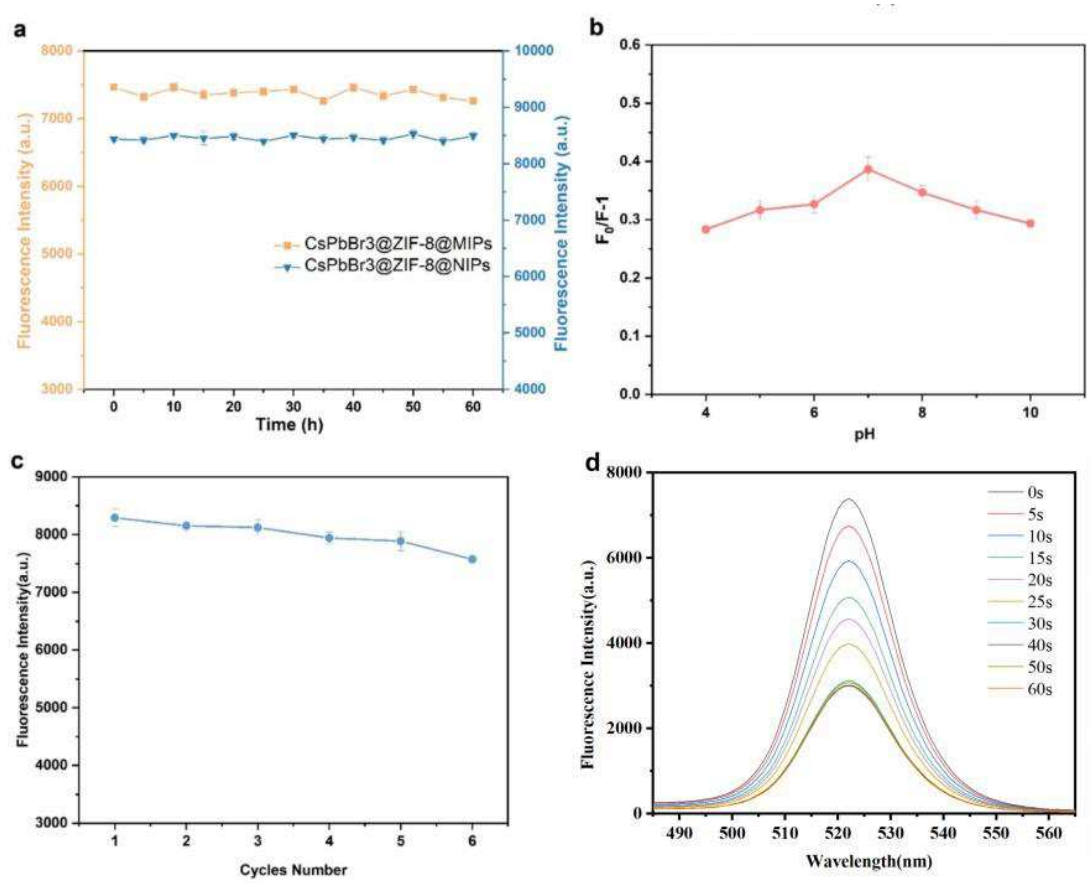


Fig. 5. Fluorescence intensity stabilities of $CsPbBr_3$@ZIF-8@MIPs and $CsPbBr_3$@ZIF-8@NIPs (a). Effect of pH value on fluorescence intensity of $CsPbBr_3$@ZIF-8@MIPs (b). The durability of $CsPbBr_3$@ZIF-8@MIPs which was examined through six binding-desorption cycles (c).Dynamic fluorescent analysis detection time of CsPbBr3@ZIF-8@MIPs to DA (200 nM) within 60s(d)

Application in Clinical Serum Samples. Serum samples were collected from five healthy adults and seven Parkinson's disease (PD) patients at Shanghai Tenth People's Hospital. The serum was centrifuged to remove proteins, and the resulting supernatant was then filtered through a 0.22 μm organic membrane to obtain the processed serum. The isolated serum was added with 0.3 mg/L $CsPbBr_3$@ZIF-8@MIPs, then fluorescence measurements were conducted. For the detection of healthy adults' samples, we used HPLC results as the gold standard to evaluate the accuracy and calculate the recovery rates of $CsPbBr_3$@ZIF-8@MIPs. The results show that recovery values ranged from 96.83% to 109.72% (Figure S1 and Table S1), which are relatively high compared to those reported in previous studies (Table S3), with relative standard deviations (RSDs) below 5%. Furthermore, as illustrated in Fig. 6, the application of $CsPbBr_3$@ZIF-8@MIPs for detecting DA levels in serum samples from healthy individuals and Parkinson's patients (refer to Table S2 for

detailed information) revealed significant differences between the two groups. Importantly, the observed significant disparity in DA levels between healthy controls and PD patients aligns well with the established pathophysiological role of dopaminergic dysfunction in Parkinson's disease, underscoring the clinical relevance of this sensing platform for early diagnostic screening.These findings indicate that the $CsPbBr_3$@ZIF-8@MIPs may provide a valuable tool for accurate analysis of DA and offer new methods for the detection of Parkinson's.

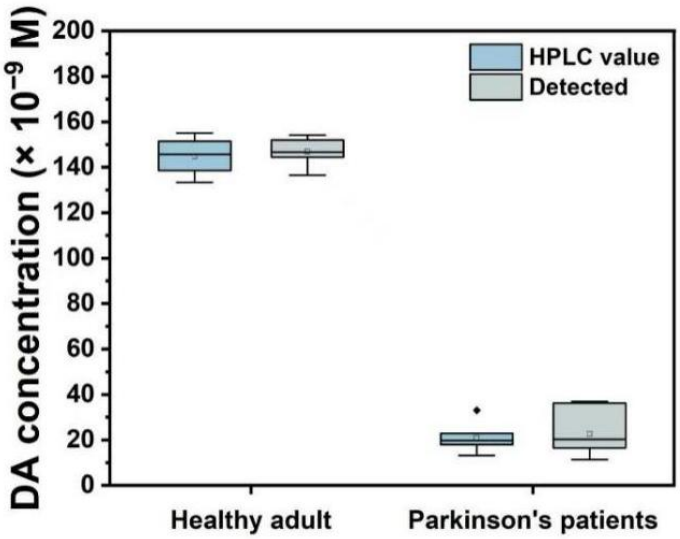


Fig. 6. Comparison of serum DA levels in healthy individuals and Parkinson's disease patients by using $CsPbBr_3$@ZIF-8@MIPs.

Conclusion

In summary, a novel surface-imprinted fluorescent sensor $CsPbBr_3$@ZIF-8@MIPs was successfully developed for highly selective and sensitive detection of dopamine. The ZIF-8 shell significantly improves the aqueous stability of perovskite quantum dots, and the MIP layer ensures excellent specificity. The sensor exhibits a low LOD of 4.85 nM, a linear range of 5–400 nM, rapid response within 30 s, and good reusability(13 measurements, Figure S1). It was successfully applied to DA detection in human serum with high recoveries and good agreement with HPLC. This strategy provides a reliable platform for DA analysis and can be extended to the sensing of other biomolecules, showing great potential for clinical diagnosis and biomedical applications.

Author Contributions

Conceptualization, Writing original draft, Investigation, Validation, Methodology: Yaowei Qin, Junpeng Yang; Assistant for methodology: Yijie Zhu; Clinical medical guidance: Zhuanxi Zhang; Conceptualization, Investigation, Writing - review & editing, Supervision, Funding acquisition: Jixiang Wang, Jingjing Xu and Yue Ma.

Disclosures

Funding Declaration: The authors acknowledge the National Natural Science Foundation of China (Nos. 32471513, 22478164). Y. Zhu and J.Xu thanks the Cultivation grant for clinical and basic integration research of Shanghai Tenth People's Hospital (No. SYYYRH2025009).

Artificial Intelligence (AI): Artificial Intelligence (AI) tools were not used.

Ethical approval： These samples were collected at Shanghai Tenth People's Hospital (Ethics Approval No.: 24KN106), with a total of five tubes obtained. In accordance with the protocol approved by our Institutional Review Board, all procedures involving human participants were conducted in accordance with the 1964 Declaration of Helsinki and its later amendments.

References

[1] O. Garritsen, E. van Battum, L. Grossouw, R. Pasterkamp, Development, wiring and function of dopamine neuron subtypes, Nat Rev Neurosci, 24(2023) 134–52, http://dx.doi.org/10.1038/s41583-022-00669-3.

[2] B. Conio, M. Martino, P. Magioncalda, A. Escelsior, M. Inglese, M. Amore, et al., Opposite effects of dopamine and serotonin on resting-state networks: review and implications for psychiatric disorders, Mol Psychiatr, 25(2020) 82–93, http://dx.doi.org/10.1038/s41380-019-0406-4.

[3] D. Weintraub, D. Aarsland, K. Chaudhuri, R. Dobkin, A. Leentjens, M. Rodriguez-Violante, et al., The neuropsychiatry of Parkinson's disease: advances and challenges, Lancet Neurol, 21(2022) 89–102, http://dx.doi.org/10.1016/s1474-4422(21)00330-6.

[4] M. Ganesana, S. Lee, Y. Wang, B. Venton, Analytical Techniques in Neuroscience: Recent Advances in Imaging, Separation, and Electrochemical Methods, Anal Chem, 89(2017) 314–41, http://dx.doi.org/10.1021/acs.analchem.6b04278.

[5] Z. Xu, X. He, H. Luo, L. Xu, N. Li, Tailoring Efficient Fluorogenic Tactic for Ultrasensitive Detection of Dopamine in Urine and Rat Brain through Real-Time and In Situ Formation of High-Performance Fluorophore, Anal Chem, 95(2023) 15965–74,

http://dx.doi.org/10.1021/acs.analchem.3c03035.
[6] V. Kumar, H. Kim, B. Pandey, T. James, J. Yoon, E. Anslyn, Recent advances in fluorescent and colorimetric chemosensors for the detection of chemical warfare agents: a legacy of the 21st century, Chem Soc Rev, 52(2023) 663–704,
http://dx.doi.org/10.1039/d2cs00651k.
[7] C. Liu, X. Lin, J. Liao, M. Yang, M. Jiang, Y. Huang, et al., Carbon dots-based dopamine sensors: Recent advances and challenges, Chin Chem Lett, 35(2024) 9,
http://dx.doi.org/10.1016/j.cclet.2024.109598.
[8] W. Ling, X. Shang, C. Yu, C. Li, K. Xu, L. Feng, et al., Miniaturized Implantable Fluorescence Probes Integrated with Metal-Organic Frameworks for Deep Brain Dopamine Sensing, ACS Nano, 18(2024) 10596–608,
http://dx.doi.org/10.1021/acsnano.4c00632.
[9] R. Sheng, Y. Liu, T. Cai, R. Wang, G. Yang, T. Wen, et al., Ultrafine FeCuAgCeGd-based high-entropy nanozyme: Preparation, catalytic mechanism, and point-of-care detection of dopamine in human serum, Chem Eng J, 485(2024) 10,
http://dx.doi.org/10.1016/j.cej.2024.149913.
[10] W. Shi, L. Zeng, R. He, X. Han, Z. Guan, M. Zhou, et al., Near-unity NIR phosphorescent quantum yield from a room-temperature solvated metal nanocluster, Science, 383(2024) 326–30,
http://dx.doi.org/10.1126/science.adk6628.
[11] X. Wu, Y. Jing, H. Zhong, In Situ Fabricated Perovskite Quantum Dots: From Materials to Applications, Adv Mater, 37(2025) 15,
http://dx.doi.org/10.1002/adma.202412276.
[12] X. Wu, H. Ji, X. Yan, H. Zhong, Industry outlook of perovskite quantum dots for display applications, Nat Nanotechnol, 17(2022) 813–6,
http://dx.doi.org/10.1038/s41565-022-01163-8.
[13] Y. Bai, M. Hao, S. Ding, P. Chen, L. Wang, Surface Chemistry Engineering of Perovskite Quantum Dots: Strategies, Applications, and Perspectives, Adv Mater, 34(2022) 35,
http://dx.doi.org/10.1002/adma.202105958.
[14] X. Li, S. Aftab, M. Mukhtar, F. Kabir, M. Khan, H. Hegazy, et al., Exploring Nanoscale Perovskite Materials for Next-Generation Photodetectors: A Comprehensive Review and Future Directions, Nano-Micro Lett, 17(2025) 63,
http://dx.doi.org/10.1007/s40820-024-01501-6.
[15] J. Chen, S. Chen, X. Liu, D. Zhu, B. Cai, X. Luo, et al., Molecule-induced ripening control in perovskite quantum dots for efficient and stable light-emitting diodes, Sci Adv, 11(2025) 10,
http://dx.doi.org/10.1126/sciadv.ads7159.
[16] S. Song, Y. Lv, B. Cao, W. Wang, Surface Modification Strategy Synthesized CsPbX3 Perovskite Quantum Dots with Excellent Stability and Optical Properties in Water, Adv Funct Mater, 33(2023) 7,
http://dx.doi.org/10.1002/adfm.202300493.
[17] C. Mi, G. Gee, C. Lander, D. Shin, M. Atteberry, N. Akhmedov, et al., Towards non-blinking and photostable perovskite quantum dots, Nat Commun, 16(2025) 13,
http://dx.doi.org/10.1038/s41467-024-55619-7.
[18] Z. Han, K. Wang, R. Liang, Y. Guo, Y. Yang, M. Wang, et al., Modular Construction of Multivariate Metal-Organic Frameworks for Luminescent Sensing, J Am Chem Soc, 147(2025)

3866–73,
http://dx.doi.org/10.1021/jacs.4c17248.
[19] S. Wang, R. Gao, M. Zheng, X. Zhang, X. Cheng, Y. Xu, et al., Highly selective ppb-level Cl2 sensor at room temperature based on ZIF-8 coated MIL-68(In)-derived hexagonal tubes, Chem Eng J, 507(2025) 10,
http://dx.doi.org/10.1016/j.cej.2025.160610.
[20] M. Song, J. Xing, H. Cai, X. Gao, C. Li, C. Liu, et al., Pomegranate-Bionic Encapsulating Horseradish Peroxidase Using Dopamine Flexible Scaffold-Coated Multishell Porous ZIF-8 To Enhance Immunochromatographic Diagnosis, ACS Nano, 17(2023) 10748–59,
http://dx.doi.org/10.1021/acsnano.3c02164.
[21] B. Bui, A. Mier, K. Haupt, Molecularly Imprinted Polymers as Synthetic Antibodies for Protein Recognition: The Next Generation, Small, 19(2023) 17,
http://dx.doi.org/10.1002/smll.202206453.
[22] Y. Li, L. Luo, Y. Kong, S. George, Y. Li, X. Guo, et al., A Point-of-Care Sensing Platform for Multiplexed Detection of Chronic Kidney Disease Biomarkers Using Molecularly Imprinted Polymers, Adv Funct Mater, 34(2024) 13,
http://dx.doi.org/10.1002/adfm.202316865.
[23] S. Jeon, S. Kim, G. Heo, H. Heo, S. Chae, Y. Kwon, et al., A Wearable Electrochemical Biosensor for Salivary Detection of Periodontal Inflammation Biomarkers: Molecularly Imprinted Polymer Sensor with Deep Learning Integration, Adv Sci, 12(2025) 18,
http://dx.doi.org/10.1002/advs.202509658.
[24] X. He, Y. Wang, Q. Xue, W. Qian, G. Li, Q. Li, Molecularly imprinted MOF nanozymes: Demonstration of smartphone-integrated dual-mode platform for ratiometric fluorescent/ colorimetric detection of chloramphenicol, Food Chem X, 26(2025) 10,
http://dx.doi.org/10.1016/j.fochx.2025.102322.
[25] B. Li, X. Liao, L. Wang, Y. Chen, Molecularly imprinted polymer coated Eu-BCA MOF for highly selective detection of Zearalenone in corn oil, Food Chem, 489(2025) 11,
http://dx.doi.org/10.1016/j.foodchem.2025.144872.
[26] L. Zhang, M. Shen, Z. Li, F. Meng, J. Wang, A. Li, et al., A Dual-Mode Sensor Based on Surface Molecularly Imprinted Metal-Organic Framework for the Highly Accurate and Selective Detection of Tetracycline, Sens Actuator B-Chem, 432(2025) 9,
http://dx.doi.org/10.1016/j.snb.2025.137445.
[27] M. Garg, N. Pamme, Strategies to remove templates from molecularly imprinted polymer (MIP) for biosensors, Trac-Trends Anal Chem, 170(2024) 8,
http://dx.doi.org/10.1016/j.trac.2023.117437.
[28] D. Li, X. Zong, Y. Ding, Y. Zhao, S. Wang, A novel sandwich-type fluorescent sensor for the selective and sensitive detection of ellagic acid based on boronate affinity oriented imprinting and silver nanoparticle-enhanced fluorescence of boronic acid-modified CdTe quantum dots, Food Chem, 493(2025) 12,
http://dx.doi.org/10.1016/j.foodchem.2025.145936.
[29] N. Hemed, S. Leal-Ortiz, E. Zhao, N. Melosh, On-Demand, Reversible, Ultrasensitive Polymer Membrane Based on Molecular Imprinting Polymer, ACS Nano, 17(2023) 5632–43,
http://dx.doi.org/10.1021/acsnano.2c11618.
[30] C. Zhou, X. Xi, X. Liu, W. Wen, X. Zhang, Z. Wu, et al., In situ detection of dopamine in

single living cells by molecularly imprinted polymer-functionalized nanoelectrodes, Biosens Bioelectron, 257(2024) 9,
http://dx.doi.org/10.1016/j.bios.2024.116332.
[31] V. Sliesarenko, U. Bren, A. Lobnik, Fluorescence based dopamine detection, Sensors and Actuators Reports, 7(2024) 100199,
https://dx.doi.org/https://doi.org/10.1016/j.snr.2024.100199

[32] L. Pan, F. Yang, S. Xu, D. Lin, C. Jiang, Fluorescence sensing probe based on functionalized mesoporous MOFs for non-invasive and detection of dopamine in human fluids, Talanta, 278(2024) 126356,
https://dx.doi.org/https://doi.org/10.1016/j.talanta.2024.126356

[33] A. Palta, D. Singla, K. Paul, V. Luxami, Coumarin-Pyrazole Based Fluorescent Sensor for Selective Detection of Dopamine in Aqueous Medium, ChemistrySelect, 8(2023) e202301864, https://dx.doi.org/https://doi.org/10.1002/slct.202301864

[34] M. Manikandan, G.L. Priya, E. Manikandan, V. Sethumadhavan, ZnO nanoparticle-enhanced electrochemical sensor utilizing moringa oleifera leaf extract for real-time dopamine detection, Journal of Inorganic and Organometallic Polymers and Materials, 34(2024) 2153–62, https://dx.doi.org/https://doi.org/10.1007/s10904-023-02955-8

[35] N. Mintz Hemed, S. Leal-Ortiz, E.T. Zhao, N.A. Melosh, On-demand, reversible, ultrasensitive polymer membrane based on molecular imprinting polymer, ACS Nano, 17(2023) 5632–43, https://dx.doi.org/https://doi.org/10.1021/acsnano.2c11618

Supplementary Files

This is a list of supplementary files associated with this preprint. Click to download.

- Table.docx
- SupplementaryMaterial.docx